Midbody proteins display distinct temporal dynamics during cytokinesis

Ella F.J. Halcrow[#], Riccardo Mazza[#], Anna Diversi, Anton Enright and Pier Paolo D'Avino[*]

Department of Pathology, University of Cambridge, Tennis Court Road, Cambridge, CB2 1QP, UK

[#]These two authors contributed equally

*Correspondence to: Pier Paolo D'Avino, email: ppd21@cam.ac.uk

Abstract

The midbody is an organelle that forms between the two daughter cells during cytokinesis. It co-ordinates the abscission of the nascent daughter cells and is composed of a multitude of proteins that are meticulously arranged into distinct temporal and spatial localization patterns. However, very little is known about the mechanisms that regulate the localization and function of midbody proteins. Here, we analyzed the temporal and spatial profiles of key midbody proteins during mitotic exit under normal conditions and after treatment with drugs that affect phosphorylation and proteasome-mediated degradation to decipher the impacts of post-translational modifications on midbody protein dynamics. Our results highlighted that midbody proteins show distinct spatio-temporal dynamics during mitotic exit and cytokinesis that depend on both ubiquitin-mediated proteasome degradation and phosphorylation/de-phosphorylation. They also identified two discrete classes of midbody proteins: 'transient' midbody proteins -including Anillin, Aurora B and PRC1- which rapidly accumulate at the midbody after anaphase onset and then slowly disappear, and 'stable' midbody proteins -including CIT-K, KIF14 and KIF23- which instead persist at the midbody throughout cytokinesis and also post abscission. These two classes of midbody proteins display distinct interaction networks with ubiquitylation factors, which could potentially explain their different dynamics and stability during cytokinesis.

Keywords: cytokinesis, midbody, phosphorylation, protein dynamics, ubiquitylation.

1. Introduction

Proper execution of cell division regulates growth, development, and reproduction by controlling the partition of genomic and cytoplasmic contents between the two nascent daughter cells. Because of the inaccessibility of the chromatin compacted into chromosomes gene transcription is severely limited during mitosis. Consequently, the vast majority of mitotic processes are regulated by reversible PTMs, including phosphorylation and ubiquitylation, which are mediated by opposing PTM enzymes (e.g., kinases vs. phosphatase and ubiquitin ligases vs. hydrolases) [1,2]. These PTMs control the intricate and finely tuned signals and protein-protein interaction networks that are responsible for the assembly of the mitotic spindle and chromosome alignment in prometaphase and metaphase, and chromosome segregation and daughter cell separation during mitotic exit and cytokinesis. Once chromosomes are properly aligned at the metaphase plate, anaphase onset is triggered by the activation of an E3 ubiquitin ligase, the anaphase promoting complex/cyclosome (APC/C), through its interaction with the cofactor Cdc20 [3]. APC/C^{Cdc20} then targets several proteins for destruction by the 26S proteasome, including cyclin B, which in turn leads to the inactivation of its cyclin-dependent kinase 1 (CDK1) partner. CDK1 inactivation is accompanied by increased activity of PP1 and PP2A serine/threonine phosphatases and changes in the distribution of other serine/threonine mitotic kinases, including Polo-like kinase 1 (PLK1) and Aurora B (AURKB), the kinase component of the chromosomal passenger complex (CPC) [4-9]. Together, these events lead to complex changes in the phosphorylation profiles and activity of a multitude of proteins that propel a remarkable re-organization of the cytoskeleton [10]. Initially, cells determine the position of the cleavage furrow through signals generated by the spindle microtubules (MTs), which are re-organized into an array of antiparallel and interdigitating MTs known as the central spindle. Spindle MTs also promote furrow ingression, which is driven by the assembly and constriction of an actomyosin contractile ring. During furrow ingression, the contractile ring compacts the central spindle and the two daughter cells remain connected by an intercellular bridge, which contains at its center an organelle, the midbody, composed of a multitude of proteins that have diverse functions (Fig. 1A) [11,12]. Some midbody proteins are former components of the contractile ring and central spindle, while others are specifically recruited during the slow midbody maturation process that ultimately leads to the abscission of the two daughter cells [13,14]. All these proteins are arranged in a very precise and stereotyped spatial pattern along the midbody [15], which depends on the multifunctional protein Citron kinase (CIT-K) [16-18]. The proper localization,

77 regulation and interactions of all these proteins are essential for the execution of abscission
78 and to prevent incorrect genome segregation [14]. In addition, recent studies have revealed
79 that the midbody also has important functions after cell division. Following abscission, the
80 midbody remnants can be either reabsorbed by one of the daughter cells or released into the
81 extracellular environment and then eventually internalized by another cell [19]. These post-
82 mitotic midbody remnants have been implicated in disparate biological processes, including
83 cell fate, pluripotency, apical-basal polarity, tissue organization, cell proliferation, cancer, and
84 cilium and lumen formation [20]. Finally, some midbody proteins have been linked to brain
85 development and microcephaly [21]. However, despite the evidence of the involvement of the
86 midbody in these important processes, our understanding of the mechanisms that regulate
87 its formation and functions are still very limited. In this study, we report that midbody proteins
88 show distinct spatio-temporal dynamics that identify two general classes: (i) 'transient'
89 midbody proteins, including Anillin (ANLN), AURKB, and protein regulator of cytokinesis 1
90 (PRC1), which rapidly accumulate at the midbody after anaphase onset, but then slowly
91 disappear; and (ii) 'stable' midbody proteins, including CIT-K, and the kinesins KIF14 and
92 KIF23/MKLP1, which instead persist to the midbody for much longer, even in post-abscission
93 midbodies. Furthermore, we present evidence that these different dynamics appears to be
94 regulated by both phosphorylation and ubiquitylation.
95
96 **2. Materials and Methods**
97 *2.1 Cell culture and treatments*
98 HeLa Kyoto were maintained in DMEM (Sigma) containing 10% Fetal Bovine Serum (Sigma)
99 and 1% pennicillin/streptomycin (Invitrogen) at 37°C and 5% CO_2. HeLa cell lines stably
100 expressing GFP-tagged transgenes were described previously [11] and cultured in the same
101 medium with the addition of appropriate selection antibiotics (puromycin and/or G418).
102 For RNA interference the following siRNAs were used: scrambled sequence control: 5'-
103 AACGUACGCGGAAUACUUCGA-3', Anillin (ANLN): 5'-GUAUCGAAACCAAUUGUGAAGUCAA-3',
104 KIF23/MKLP1: 5'-GCAGUCUUCCAGGUCAUCU-3', using Lipofectamine RNAiMAX
105 (ThermoFisher) following the manufacturer's instructions.
106 To synchronize HeLa Kyoto cells at different stages of mitosis, we used a thymidine-
107 nocodazole block and release procedure essentially as described [11]. Cells were first arrested
108 in S phase by the addition of 2 mM thymidine (Sigma-Aldrich) for 19 h, washed twice with
109 phosphate-buffered saline (PBS) and released for 5 h in fresh complete medium. Cells were

110 then cultured for additional 13 h in fresh complete medium containing 50 ng/ml nocodazole
111 (Sigma-Aldrich) and then harvested by mitotic shake-off. Mitotic cells were washed five times
112 with PBS, and released in fresh medium containing either one of the following drugs: 10 µM
113 MG132 (proteasome inhibitor, Sigma), 50 nM okadaic acid (PP1 and PP2A inhibitor,
114 Calbiochem), 2 µM tautomycetin (PP1 inhibitor, TOCRIS), 2 µM ZM447439 (AURKB inhibitor,
115 TOCRIS) or the DMSO solvent as control. Cells were then harvested by centrifugation and
116 frozen in dry ice.
117
118 *2.2 Fluorescence microscopy*
119 HeLa cells were grown on microscope glass coverslips (Menzel-Gläser) and fixed in either
120 PHEM buffer (60 mM Pipes, 25 mM Hepes pH 7, 10 mM EGTA, 4 mM $MgCl_2$, 3.7% [v/v]
121 formaldheyde) for 12 min at room temperature or in ice-cold methanol for 10 min at -20°C.
122 They were then washed three times for 10 min with PBS and incubated in blocking buffer (PBS,
123 0.5% [v/v] Triton X-100 and 5% [w/v] BSA) for 1 h at room temperature. Coverslips were
124 incubated overnight at 4°C with the primary antibodies indicated in the figure legends, diluted
125 in PBT (PBS, 0.1% [v/v] Triton X-100 and 1% [w/v] BSA). The day after, coverslips were washed
126 twice for 5 min in PBT, incubated with secondary antibodies diluted in PBT for 2h at RT and
127 then washed twice with PBT and once with PBS. Coverslips were mounted on SuperFrost
128 Microscope Slides (VWR) using VECTASHIELD Mounting Medium containing DAPI (Vector
129 Laboratories). Images were acquired using a Zeiss Axiovert epifluorescence microscope
130 equipped with MetaMorph software. Fiji [22] was used to generate maximum intensity
131 projections, which were adjusted for contrast and brightness and assembled using Photoshop.
132
133 *2.3 Western blot*
134 Cells were centrifuged, resuspended in phosphate buffer saline (PBS) and then an equal
135 volume of 2x Laemmli buffer was added. Samples were then boiled for 10 min and stored at
136 -20°C. Proteins were separated by SDS PAGE and then transferred onto PVDF membrane
137 (Immobilon-P) at 15V for 1 hour. Membranes were blocked overnight at 4°C in PBS + 0.1%
138 (v/v) Tween (PBST) with 5% (v/v) dry milk powder. After blocking, membranes were washed
139 once with PBST and then incubated with the appropriate primary antibody diluted in PBST +
140 3% (v/v) BSA (Sigma) for 2 hours at RT. Membranes were washed 3x5 minutes in PBST and
141 then incubated with HRPA-conjugated secondary antibodies in PBST + 1% BSA for 1 hour at
142 room temperature. After further 3x5 min washes in PBST, the signals were detected using the

143 ECL West Pico substrate (ThermoFisher) and chemiluminescent signals were acquired below
144 saturation levels using a G:BOX Chemi XRQ (Syngene) and quantified using Fiji [22].
145
146 *2.4 Antibodies*
147 The following antibodies were used in this study: rabbit polyclonal anti-ANLN (Abcam,
148 ab154337, dilutions for WB, 1:2000, for IF 1:200), mouse monoclonal anti-Aurora B (clone
149 AIM-1, BD Transduction Laboratories, 611082 dilutions for WB 1:2000, for IF 1:100), mouse
150 monoclonal anti-CIT-K (BD Transduction Laboratories, 611377, dilutions for WB 1:1500, for IF
151 1:200), mouse monoclonal anti-cyclin B1 (clone GNS1, Santa Cruz, sc-245 dilution for WB
152 1:2000), rabbit monoclonal anti-MKLP1 (Abcam ab174304, dilutions for WB 1:5000, for IF
153 1:800), rabbit polyclonal anti-KIF20A/MKLP2 (a kind gift of T.U. Mayer [23], dilution for both
154 WB and IF 1:1000) , mouse monoclonal anti-PRC1 (clone C-1, Santa Cruz, sc-376983 dilutions
155 for WB 1:5000, for IF 1:100), rabbit polyclonal anti-phospho-histone H3 pS10 (Merck, 06-570
156 dilution for WB 1:10000), mouse monoclonal anti α-tubulin (clone DM1A, Sigma, T9026
157 dilutions for WB 1:20000, for IF 1:2000), rabbit polyclonal anti-β-tubulin (Abcam, ab6046
158 dilutions for WB 1:5000, for IF 1:400). Peroxidase and Alexa-fluor conjugated secondary
159 antibodies were purchased from Jackson Laboratories and ThermoFisher, respectively.
160
161 *2.5 Time-lapse imaging*
162 For time-lapse experiments, HeLa cells expressing the different GFP-tagged proteins were
163 plated on an open μ-Slide with 8 wells (Ibidi, 80826) in complete medium containing 0.5 μM
164 SiR-DNA dye (SpiroChrome). Images were acquired on a Leica TCS SP8 Inverted Microscope
165 with a 40x/1.30 NA HC Plan APO CS2 - OIL DIC objective and argon laser power set at 80%. The
166 Application Suite X software (LAS-X; Leica) for multidimensional image acquisition was used.
167 Specimens were maintained at 37°C and 5% CO_2 via a chamber, and z-series of ten, 1-μm
168 sections were captured at 2 min intervals. All images were processed using Fiji [22] to generate
169 maximum intensity projections, to adjust for brightness and contrast, and to create the final
170 movies. The fluorescence intensity values shown in Figure 3 were measured from whole cells
171 (I_C) or midbodies (I_M) at the different time points indicated using Fiji [22]. A background
172 intensity value, measured at the same time point and from an identically sized area, was
173 subtracted from each value.
174
175 *2.6 Computational and statistical analyses*

176 To generate the ubiquitylation midbody sub-network, we searched our midbody interactome
177 dataset [11] for proteins whose Uniprot protein names field contained the term 'ubiquitin' via
178 grep in the Unix command line. This generated an initial dataset that was subsequently
179 manually curated to eliminate proteins that were not directly involved in ubiquitylation. The
180 final list of 86 proteins (Table S1) was entered into a raw tab-delimited text file and then
181 imported into Cytoscape to generate the network shown in Figure 4.
182 Prism 9 (GraphPad) and Excel (Microsoft) were used for statistical analyses and to prepare
183 graphs.
184

185 **3. Results and Discussion**

186 *3.1 Midbody protein distribution changes during midbody maturation.*

187 Immuno-fluorescence and electron microscopy studies have indicated that the midbody can
188 be divided in three major regions: (i) the midbody ring, containing former contractile ring
189 components like Anillin (ANLN) and CIT-K; (ii) the midbody central core, marked by central
190 spindle proteins such as the centralspindlin complex (an heterotetramer composed of two
191 subunits of the kinesin KIF23/MKLP1 and two molecules of RacGAP1); and (iii) the midbody
192 arms, which flank the midbody core and where AURKB and the kinesin KIF20A/MKLP2
193 accumulate (Fig. 1A) [13,15,18]. However, the midbody is not a static structure, it undergoes a
194 series of morphological changes during the late stages of cytokinesis, in a process known as
195 midbody maturation. After completion of furrow ingression, two symmetric constrictions
196 form at both sides of the midbody ring, making the midbody look similar to a 'bow tie' (Fig. 1).
197 Subsequently, the microtubule bundles become progressively thinner and ultimately a distinct
198 abscission site appears usually first at one side of the midbody ring [13]. These changes in
199 midbody architecture are often reflected by changes in the distribution of midbody proteins.
200 For example, after completion of furrow ingression ANLN and CIT-K both localize to the
201 midbody ring -albeit ANLN display a broader distribution (Fig. 1B and C)- but, whilst CIT-K
202 maintains a ring-like distribution and persists in post-abscission midbody remnants (Fig. 3C)
203 [17,18], ANLN accumulates to the secondary constriction sites and then disappears from the
204 midbody before abscission (Fig. 1C) [24]. AURKB localizes to the midbody arms throughout
205 midbody maturation, although its accumulation slowly decreases during midbody maturation,
206 similarly to ANLN. The kinesin KIF23/MKLP2 localizes to the midbody core after furrow
207 ingression and then, starting from the 'bow tie' stage, it forms two juxtaposed discs and
208 persists in post-abscission midbodies like CIT-K (Fig. 1C and Fig 3D).

209 Previous studies have indicated that CIT-K plays an important role in establishing and
210 maintaining the orderly distribution of these midbody proteins, possibly through its direct
211 interaction with some midbody components, including ANLN, AURKB, KIF14 and KIF23/MKLP1
212 [11,16-18,25,26]. Nevertheless, we still lack sufficient knowledge of the underlying mechanisms
213 that control the dynamics and stability of midbody proteins during and after cytokinesis.
214
215 *3.2 Midbody proteins display different expression profiles during mitotic exit and cytokinesis*
216 To get a detailed understanding of the dynamics of midbody proteins, we first analyzed their
217 expression profiles by Western blot in synchronized cells as they exited mitosis. HeLa cells
218 were synchronized in prometaphase by thymidine/nocodazole block and then released to
219 analyze the levels of midbody proteins (Fig. 2A and B). The specificity of the antibodies used
220 in this analysis has been previously validated [11,18,27], apart from the anti-ANLN and a new
221 anti-KIF23/MKLP1 antibody, which we validated using siRNA-mediated depletion
222 (Supplementary Fig. S1). The levels of cyclin B and histone H3 phosphorylated at S10 (pH3),
223 which both decrease after anaphase onset, were used to monitor mitotic exit. Cyclin B levels
224 dropped significantly (more than 80%) 60 min after release from nocodazole, indicating that
225 the vast majority of cells had exited mitosis at this time point. The levels of KIF14 and
226 KIF23/MKLP1 remained relatively stable after nocodazole release, whereas the levels of all
227 other midbody proteins decreased during mitotic exit (Fig. 2A and 2B). ANLN showed a profile
228 very similar to that of Cyclin B, while the levels of all the other midbody proteins analyzed,
229 AURKB, CIT-K, KIF20A/MKLP2 and PRC1 decreased more slowly, in parallel with pH3.
230 As mentioned before, mitotic exit is triggered by ubiquitin-mediated protein degradation and
231 regulated by phosphorylation/dephosphorylation of cytokinesis proteins. Therefore, to
232 understand which PTM(s) might be involved in regulating the level of midbody proteins, we
233 incubated HeLa cells for a short period of time (one hour) with 4 different inhibitors – the
234 proteasome inhibitor MG132, okadaic acid to inhibit both PP1 and PP2A phosphatases, the
235 PP1-specific inhibitor tautomycetin [28], and the AURKB inhibitor ZM447439 [29] – starting
236 from 45 minutes after release from nocodazole, when most cells should be already in, or about
237 to enter anaphase. The analysis from this indicated that midbody proteins can be divided into
238 three main groups on the basis of their response to drug treatments (Fig, 2C, 2D and
239 Supplementary Fig. S2). In one group, ANLN and PRC1 profiles mimicked that of cyclin B, as
240 they were stabilized after treatment with MG132 (Fig. 2C, 2D and Supplementary Fig. S2A).
241 This is consistent with the evidence that all these proteins are ubiquitinated to be degraded

242 during mitotic exit [30-32]. The levels of all these three proteins also appeared to decline faster
243 after incubation with the AURKB inhibitor ZM447439 (Fig. 2C, 2D and Supplementary Fig. S2A),
244 which could either reflects a more rapid mitotic exit triggered by AURKB inhibition or indicate
245 that AURKB activity is required for the stability of these midbody proteins in late telophase.
246 We favor the latter for two main reasons. Firstly, none of the other proteins showed a similar
247 response and secondly, ZM447439 was added 45 minutes after nocodazole release, when the
248 majority of cells were already in anaphase. A second group included AURKB and CIT-K, which
249 were also stabilized by MG132 treatment (albeit less than ANLN, cyclin B and PRC1), but their
250 levels did not change after treatment with any of the other inhibitors (Fig. 2C, 2D and
251 Supplementary Fig. S2B). These results are consistent with the role of the APC/C in the
252 degradation of Aurora kinases during mitotic exit [33], but reveal for the first time that CIT-K
253 might also be similarly targeted for degradation via ubiquitination. The final group comprises
254 the kinesins, KIF14, KIF23/MKLP1, and KIF20A/MKLP2, which do not appear to be particularly
255 affected by any of the drug treatment, with the exception of KIF23/MKLP1, whose levels are
256 higher after incubation with the two phosphatase inhibitors (Fig. 2C, 2D and Supplementary
257 Fig. S2C). This result indicates that KIF23/MKLP1 dephosphorylation might affect its stability,
258 perhaps by affecting its interaction with other midbody proteins. This is in line with our
259 previous observation that this kinesin is a PP1 substrate and PP1-mediated dephosphorylation
260 regulates its interaction with other midbody proteins, including PRC1 [11].
261 Together, these findings indicate that, in whole cells, the levels of most midbody proteins
262 decrease during mitotic exit, with the exception of some 'stable' midbody proteins such as
263 KIF14 and KIF20A. In addition, drug treatments indicate that this may be regulated by both
264 ubiquitin-mediated proteasome degradation and phosphorylation/de-phosphorylation.
265
266 *3.3 Midbody proteins display distinct dynamics during mitotic exit and cytokinesis*
267 Our western blot analyses only detected the total amount of midbody proteins in the cell.
268 Therefore, we next employed time-lapse microscopy to gain more detailed information about
269 the spatial and temporal dynamics of midbody proteins during mitotic exit and cytokinesis.
270 We selected cell lines stably expressing GFP-tagged versions of four midbody proteins
271 representative of the different profiles and responses to drug treatments observed in the
272 western blot experiments (Fig. 2): AURKB, CIT-K, KIF23/MKLP1 and PRC1 [11]. Cells were also
273 incubated with a DNA dye to identify cells in mitosis and to simultaneously visualize the
274 dynamics of chromosomes and midbody proteins. For each GFP-tagged protein, we also

275 measured fluorescence levels in the whole cell and at the central spindle/cleavage
276 furrow/midbody. AURKB and PRC1 showed very similar dynamics, as they initially
277 accumulated at the midbody, but then their levels slowly decreased and low fluorescence
278 signals were observed at the midbody 1 hour after anaphase onset (Fig. 3A, 3B and 3E; Videos
279 S1 and S2). Notably, the decrease observed at the central spindle/midbody was more rapid
280 than that observed in whole cells (Fig. 3E). By contrast, CIT-K and KIF23/MKLP1, after the initial
281 accumulation to the either the cleavage furrow (CIT-K) or central spindle (MKLP1), persisted
282 at the midbody for much longer, up to 2 hours after anaphase onset and even in post-mitotic
283 midbody (Fig. 3C-E and Videos S3 and S4).
284 These results indicate that midbody proteins can be divided into two distinct classes based on
285 their dynamics profiles: 'transient' midbody proteins, such as AURKB and PRC1, which after
286 an initial accumulation at the midbody then slowly dissipate; and 'stable' midbody proteins
287 that instead persists at the midbody both during and after cytokinesis
288
289 *3.4 Transient and stable midbody proteins display distinct interactions with ubiquitylation*
290 *factors*
291 Our findings indicated that transient and stable midbody proteins have different expression
292 and dynamics profiles (Figs, 2 and 3) and that the levels of some proteins are regulated by
293 proteasome-mediated degradation (Fig. 2). Therefore, as a first step to understand if and how
294 ubiquitylation might be involved in regulating midbody protein dynamics and/or stability, we
295 generated a midbody ubiquitylation protein-protein interaction network (interactome) by
296 extracting from our previously published midbody interactome dataset [11] proteins whose
297 full names and/or gene ontology (GO) terms in the fields biological process, cellular
298 component and molecular function, contained the term "ubiquitin" (Fig. 4 A, Table S1). From
299 this midbody interactome, we then generated two distinct sub-networks using either
300 'transient' or 'stable' midbody proteins as baits (Fig. 4B-D). We decided to include CIT-K among
301 the stable proteins, despite the evidence that its levels decline during mitotic exit (Fig. 2A, 2B)
302 and are slightly stabilized by MG132 (Fig. 2C and 2D), because time-lapse imaging clearly
303 indicated that CIT-K stably localized to the midbody during and after cytokinesis (Fig. 3C and
304 3E). Although the two networks showed considerable overlap (29 out of 76 proteins; Fig. 4B),
305 they also had distinct interactors (Fig. 4B-D). This would suggest that ubiquitylation of the two
306 different classes of midbody proteins could be differentially regulated, by specific ubiquitin
307 ligases and/or deubiquitinating enzymes (deubiquitinases, DUBs). Our observation that CIT-K

308 persists at the midbody, while its cellular levels decline during mitotic exit and are slightly
309 stabilized by proteasome inhibition, is consistent with the possibility that one or more DUBs
310 might be involved in preventing CIT-K degradation specifically at the midbody. Analysis of the
311 transient and stable midbody ubiquitylation interactomes showed that some DUBs specifically
312 associated with either transient or stable proteins (Table 1). In particular, USP7 and OTUD4
313 were pulled down only by KIF23/MKLP1 and USP10 associated specifically with the two close
314 partners CIT-K and KIF14 [16,26,34]. KIF14 was the only bait that pulled down USP36 and USP9X.
315 The three DUBs specifically found in the transient midbody ubiquitylation interactome,
316 UCHL1, USP4 and USP54 all associated with KIF20A/MKLP2, and UCHL1 also interacted with
317 PRC1. It is noteworthy that some of these DUBs have already been implicated in the regulation
318 of mitosis. For example, USP7 has been reported to regulate the spindle assembly checkpoint
319 component BUB3 and the three mitotic kinases Aurora A, CDK1, and PLK1 [35-38]. Moreover,
320 USP9X has been shown to antagonize the APC/C and to regulate the localization of the CPC
321 component Survivin [39,40].
322 In conclusion, our analysis suggests that these specific interactions between DUBs and stable
323 or transient midbody proteins could potentially explain, at least in part, the different dynamics
324 and stability of these midbody proteins during cytokinesis. Future studies aimed at defining
325 the molecular mechanisms underpinning the stability and dynamics of midbody proteins will
326 undoubtedly help us to understand how this organelle regulates abscission and other
327 important biological processes, including cell fate, cell proliferation, tissue architecture and
328 brain development.
329
330 **Author Contributions:** Conceptualization, P.P.D., investigation, A.D., E.F.J.H., R.M. and P.P.D.;
331 software, A.E.; formal analysis, A.E. and P.P.D.; writing—original draft preparation, P.P.D.;
332 writing—review and editing, E.F.J.H. and P.P.D.; visualization E.F.J.H., R.M. and P.P.D.,
333 supervision, P.P.D.; project administration, P.P.D.; funding acquisition, P.P.D. All authors have
334 read and agreed to the published version of the manuscript.
335
336 **Funding:** This research was funded by a BBSRC grant to PPD (ref: BB/R001227/1). EFJH is
337 supported by a BBSRC DTP studentship and RM was supported through an exchange program
338 between the Collegio Ghislieri (University of Pavia, Italy) and St. John's College (University of
339 Cambridge, UK). AD was supported by an Erasmus traineeship program from the University of
340 Bologna (Italy).

Institutional Review Board Statement: Not applicable.

Informed Consent Statement: Not applicable.

Data Availability Statement: Not applicable.

Acknowledgments: We are very grateful to P.A. Coelho for help with time-lapse experiments.

Conflicts of Interest: The authors declare no conflict of interest.

References

1. Cuijpers, S.A.G.; Vertegaal, A.C.O. Guiding Mitotic Progression by Crosstalk between Post-translational Modifications. *Trends in biochemical sciences* **2018**, *43*, 251-268, doi:10.1016/j.tibs.2018.02.004.
2. Wieser, S.; Pines, J. The biochemistry of mitosis. *Cold Spring Harbor perspectives in biology* **2015**, *7*, a015776, doi:10.1101/cshperspect.a015776.
3. Lindon, C. Control of mitotic exit and cytokinesis by the APC/C. *Biochem Soc Trans* **2008**, *36*, 405-410, doi:10.1042/BST0360405.
4. Holder, J.; Poser, E.; Barr, F.A. Getting out of mitosis: spatial and temporal control of mitotic exit and cytokinesis by PP1 and PP2A. *FEBS Lett* **2019**, *593*, 2908-2924, doi:10.1002/1873-3468.13595.
5. Carmena, M.; Wheelock, M.; Funabiki, H.; Earnshaw, W.C. The chromosomal passenger complex (CPC): from easy rider to the godfather of mitosis. *Nat Rev Mol Cell Biol* **2012**, *13*, 789-803, doi:10.1038/nrm3474.
6. D'Avino, P.P.; Capalbo, L. New Auroras on the Roles of the Chromosomal Passenger Complex in Cytokinesis: Implications for Cancer Therapies. *Front Oncol* **2015**, *5*, 221, doi:10.3389/fonc.2015.00221.
7. Nasa, I.; Kettenbach, A.N. Coordination of Protein Kinase and Phosphoprotein Phosphatase Activities in Mitosis. *Front Cell Dev Biol* **2018**, *6*, 30, doi:10.3389/fcell.2018.00030.
8. Archambault, V.; Glover, D.M. Polo-like kinases: conservation and divergence in their functions and regulation. *Nat Rev Mol Cell Biol* **2009**, *10*, 265-275, doi:10.1038/nrm2653.
9. Fededa, J.P.; Gerlich, D.W. Molecular control of animal cell cytokinesis. *Nat Cell Biol* **2012**, *14*, 440-447, doi:10.1038/ncb2482.
10. D'Avino, P.P.; Giansanti, M.G.; Petronczki, M. Cytokinesis in animal cells. *Cold Spring Harbor perspectives in biology* **2015**, *7*, a015834, doi:10.1101/cshperspect.a015834.
11. Capalbo, L.; Bassi, Z.I.; Geymonat, M.; Todesca, S.; Copoiu, L.; Enright, A.J.; Callaini, G.; Riparbelli, M.G.; Yu, L.; Choudhary, J.S.; et al. The midbody interactome reveals unexpected roles for PP1 phosphatases in cytokinesis. *Nature communications* **2019**, *10*, 4513, doi:10.1038/s41467-019-12507-9.

384 12. Skop, A.R.; Liu, H.; Yates, J., 3rd; Meyer, B.J.; Heald, R. Dissection of the mammalian
385 midbody proteome reveals conserved cytokinesis mechanisms. *Science* **2004**, *305*,
386 61-66, doi:10.1126/science.1097931.
387 13. D'Avino, P.P.; Capalbo, L. Regulation of midbody formation and function by mitotic
388 kinases. *Semin Cell Dev Biol* **2016**, *53*, 57-63, doi:10.1016/j.semcdb.2016.01.018.
389 14. Mierzwa, B.; Gerlich, D.W. Cytokinetic abscission: molecular mechanisms and
390 temporal control. *Dev Cell* **2014**, *31*, 525-538, doi:10.1016/j.devcel.2014.11.006.
391 15. Hu, C.K.; Coughlin, M.; Mitchison, T.J. Midbody assembly and its regulation during
392 cytokinesis. *Mol Biol Cell* **2012**, *23*, 1024-1034, doi:10.1091/mbc.E11-08-0721.
393 16. Bassi, Z.I.; Audusseau, M.; Riparbelli, M.G.; Callaini, G.; D'Avino, P.P. Citron kinase
394 controls a molecular network required for midbody formation in cytokinesis. *Proc*
395 *Natl Acad Sci U S A* **2013**, *110*, 9782-9787, doi:10.1073/pnas.1301328110.
396 17. D'Avino, P.P. Citron kinase - renaissance of a neglected mitotic kinase. *J Cell Sci* **2017**,
397 *130*, 1701-1708, doi:10.1242/jcs.200253.
398 18. McKenzie, C.; Bassi, Z.I.; Debski, J.; Gottardo, M.; Callaini, G.; Dadlez, M.; D'Avino, P.P.
399 Cross-regulation between Aurora B and Citron kinase controls midbody architecture
400 in cytokinesis. *Open Biol* **2016**, *6*, 160019, doi:10.1098/rsob.160019.
401 19. Crowell, E.F.; Gaffuri, A.L.; Gayraud-Morel, B.; Tajbakhsh, S.; Echard, A. Engulfment of
402 the midbody remnant after cytokinesis in mammalian cells. *J Cell Sci* **2014**, *127*, 3840-
403 3851, doi:10.1242/jcs.154732.
404 20. Peterman, E.; Prekeris, R. The postmitotic midbody: Regulating polarity, stemness,
405 and proliferation. *J Cell Biol* **2019**, *218*, 3903-3911, doi:10.1083/jcb.201906148.
406 21. Siskos, N.; Stylianopoulou, E.; Skavdis, G.; Grigoriou, M.E. Molecular Genetics of
407 Microcephaly Primary Hereditary: An Overview. *Brain Sci* **2021**, *11*,
408 doi:10.3390/brainsci11050581.
409 22. Schindelin, J.; Arganda-Carreras, I.; Frise, E.; Kaynig, V.; Longair, M.; Pietzsch, T.;
410 Preibisch, S.; Rueden, C.; Saalfeld, S.; Schmid, B.; et al. Fiji: an open-source platform
411 for biological-image analysis. *Nat Methods* **2012**, *9*, 676-682,
412 doi:10.1038/nmeth.2019.
413 23. Hummer, S.; Mayer, T.U. Cdk1 negatively regulates midzone localization of the
414 mitotic kinesin Mklp2 and the chromosomal passenger complex. *Curr Biol* **2009**, *19*,
415 607-612, doi:10.1016/j.cub.2009.02.046.
416 24. Renshaw, M.J.; Liu, J.; Lavoie, B.D.; Wilde, A. Anillin-dependent organization of septin
417 filaments promotes intercellular bridge elongation and Chmp4B targeting to the
418 abscission site. *Open Biol* **2014**, *4*, 130190, doi:10.1098/rsob.130190.
419 25. Gai, M.; Camera, P.; Dema, A.; Bianchi, F.; Berto, G.; Scarpa, E.; Germena, G.; Di
420 Cunto, F. Citron kinase controls abscission through RhoA and anillin. *Mol Biol Cell*
421 **2011**, *22*, 3768-3778, doi:mbc.E10-12-0952 [pii], 10.1091/mbc.E10-12-0952.
422 26. Gruneberg, U.; Neef, R.; Li, X.; Chan, E.H.; Chalamalasetty, R.B.; Nigg, E.A.; Barr, F.A.
423 KIF14 and citron kinase act together to promote efficient cytokinesis. *J Cell Biol* **2006**,
424 *172*, 363-372.
425 27. Scott, S.J.; Suvarna, K.S.; D'Avino, P.P. Synchronization of human retinal pigment
426 ephitilial-1 (RPE-1) cells in mitosis. *J Cell Sci* **2020**, doi:10.1242/jcs.247940.
427 28. Mitsuhashi, S.; Matsuura, N.; Ubukata, M.; Oikawa, H.; Shima, H.; Kikuchi, K.
428 Tautomycetin is a novel and specific inhibitor of serine/threonine protein
429 phosphatase type 1, PP1. *Biochem Biophys Res Commun* **2001**, *287*, 328-331,
430 doi:10.1006/bbrc.2001.5596.
431 29. Ditchfield, C.; Johnson, V.L.; Tighe, A.; Ellston, R.; Haworth, C.; Johnson, T.; Mortlock,
432 A.; Keen, N.; Taylor, S.S. Aurora B couples chromosome alignment with anaphase by

433 targeting BubR1, Mad2, and Cenp-E to kinetochores. *J Cell Biol* **2003**, *161*, 267-280,
434 doi:10.1083/jcb.200208091, jcb.200208091 [pii].
435 30. Zhao, W.M.; Fang, G. Anillin is a substrate of anaphase-promoting
436 complex/cyclosome (APC/C) that controls spatial contractility of myosin during late
437 cytokinesis. *J Biol Chem* **2005**, *280*, 33516-33524.
438 31. Paccosi, E.; Costanzo, F.; Costantino, M.; Balzerano, A.; Monteonofrio, L.; Soddu, S.;
439 Prantera, G.; Brancorsini, S.; Egly, J.M.; Proietti-De-Santis, L. The Cockayne syndrome
440 group A and B proteins are part of a ubiquitin-proteasome degradation complex
441 regulating cell division. *Proc Natl Acad Sci U S A* **2020**, *117*, 30498-30508,
442 doi:10.1073/pnas.2006543117.
443 32. Glotzer, M.; Murray, A.W.; Kirschner, M.W. Cyclin is degraded by the ubiquitin
444 pathway. *Nature* **1991**, *349*, 132-138, doi:10.1038/349132a0.
445 33. Floyd, S.; Pines, J.; Lindon, C. APC/C Cdh1 targets aurora kinase to control
446 reorganization of the mitotic spindle at anaphase. *Curr Biol* **2008**, *18*, 1649-1658.
447 34. Watanabe, S.; De Zan, T.; Ishizaki, T.; Narumiya, S. Citron kinase mediates transition
448 from constriction to abscission through its coiled-coil domain. *J Cell Sci* **2013**, *126*,
449 1773-1784, doi:10.1242/jcs.116608.
450 35. Galarreta, A.; Valledor, P.; Ubieto-Capella, P.; Lafarga, V.; Zarzuela, E.; Munoz, J.;
451 Malumbres, M.; Lecona, E.; Fernandez-Capetillo, O. USP7 limits CDK1 activity
452 throughout the cell cycle. *EMBO J* **2021**, *40*, e99692, doi:10.15252/embj.201899692.
453 36. Giovinazzi, S.; Morozov, V.M.; Summers, M.K.; Reinhold, W.C.; Ishov, A.M. USP7 and
454 Daxx regulate mitosis progression and taxane sensitivity by affecting stability of
455 Aurora-A kinase. *Cell Death Differ* **2013**, *20*, 721-731, doi:10.1038/cdd.2012.169.
456 37. Giovinazzi, S.; Sirleto, P.; Aksenova, V.; Morozov, V.M.; Zori, R.; Reinhold, W.C.; Ishov,
457 A.M. Usp7 protects genomic stability by regulating Bub3. *Oncotarget* **2014**, *5*, 3728-
458 3742, doi:10.18632/oncotarget.1989.
459 38. Peng, Y.; Liu, Y.; Gao, Y.; Yuan, B.; Qi, X.; Fu, Y.; Zhu, Q.; Cao, T.; Zhang, S.; Yin, L.; et
460 al. USP7 is a novel Deubiquitinase sustaining PLK1 protein stability and regulating
461 chromosome alignment in mitosis. *J Exp Clin Cancer Res* **2019**, *38*, 468,
462 doi:10.1186/s13046-019-1457-8.
463 39. Skowyra, A.; Allan, L.A.; Saurin, A.T.; Clarke, P.R. USP9X Limits Mitotic Checkpoint
464 Complex Turnover to Strengthen the Spindle Assembly Checkpoint and Guard against
465 Chromosomal Instability. *Cell Rep* **2018**, *23*, 852-865,
466 doi:10.1016/j.celrep.2018.03.100.
467 40. Vong, Q.P.; Cao, K.; Li, H.Y.; Iglesias, P.A.; Zheng, Y. Chromosome alignment and
468 segregation regulated by ubiquitination of survivin. *Science* **2005**, *310*, 1499-1504,
469 doi:10.1126/science.1120160.
470

471 **Table 1**. List of deubiquitinases (DUB) identified in the midbody ubiquitylation interactome
472

Group	***Gene Name***	***Protein Name***	***Baits (MASCOT score)***	***Midbody proteome***
Common	VCP	Transitional endoplasmic reticulum ATPase (TER ATPase)	ANLN (84); AURKB (174); KIF14 (76); PRC1 (158)	Yes
	USP5	Ubiquitin carboxyl-terminal hydrolase 5	MKLP1 (41); PRC1 (83)	No
	EIF3F	Eukaryotic translation initiation factor 3 subunit F	ANLN (61); CIT-K (79); KIF14 (59); MKLP1 (73); PRC1 (136)	Yes
	USP9Y	Probable ubiquitin carboxyl-terminal hydrolase FAF-Y	KIF14 (42); KIF20A (36); MKLP1 (68)	No
	USP39	U4/U6.U5 tri-snRNP-associated protein 2	AURKB (36); CIT-K (300); PRC1 (156)	Yes
Transient-specific	UCHL1	Ubiquitin carboxyl-terminal hydrolase isozyme L1	KIF20A (30); PRC1 (392)	No
	USP54	Inactive ubiquitin carboxyl-terminal hydrolase 54	KIF20A (104)	No
	USP4	Ubiquitin carboxyl-terminal hydrolase 4	KIF20A (40)	No
Stable-specific	OTUD4	OTU domain-containing protein 4	MKLP1 (38)	No
	USP7	Ubiquitin carboxyl-terminal hydrolase 7	MKLP1 (51)	Yes
	USP10	Ubiquitin carboxyl-terminal hydrolase 10	CIT-K (59); KIF14 (126)	Yes
	USP36	Ubiquitin carboxyl-terminal hydrolase 36	KIF14 (139)	No
	USP9X	Probable ubiquitin carboxyl-terminal hydrolase FAF-X	KIF14 (50);	No

473

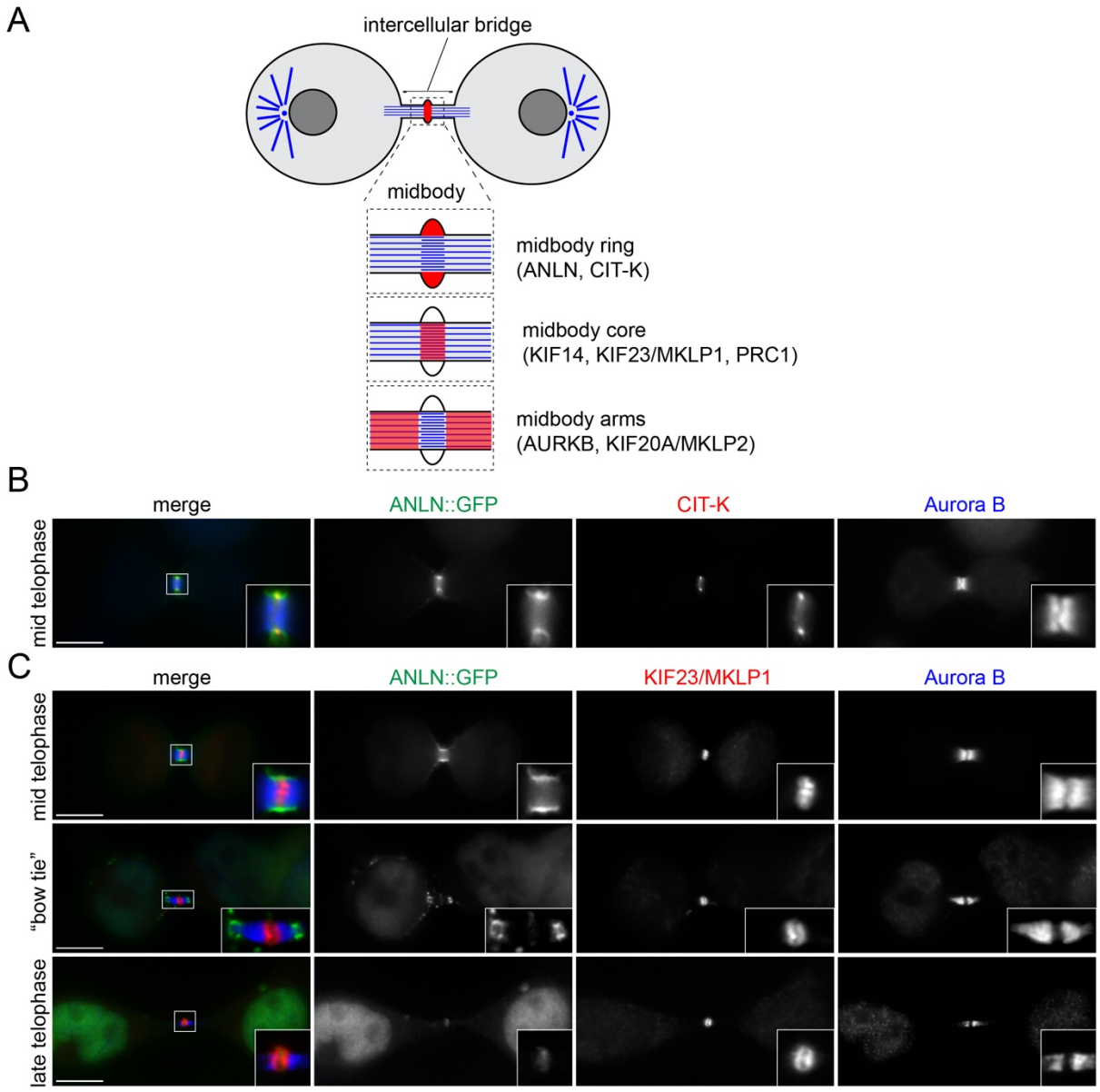

Figure 1. Changes in midbody protein distribution during its maturation. (A) Schematic diagram of the midbody showing its different regions and the localization of the proteins analyzed in this study. (B and C) HeLa cells expressing ANLN::GFP were fixed and stained to detect GFP (green in the merged panels) Aurora B (blue in the merged panels) and either CIT-K (red in the merged panel in B) or KIF23/MKLP1 (red in the merged panels in C). Insets show a 3x magnification of the midbody. Bars, 10 µm.

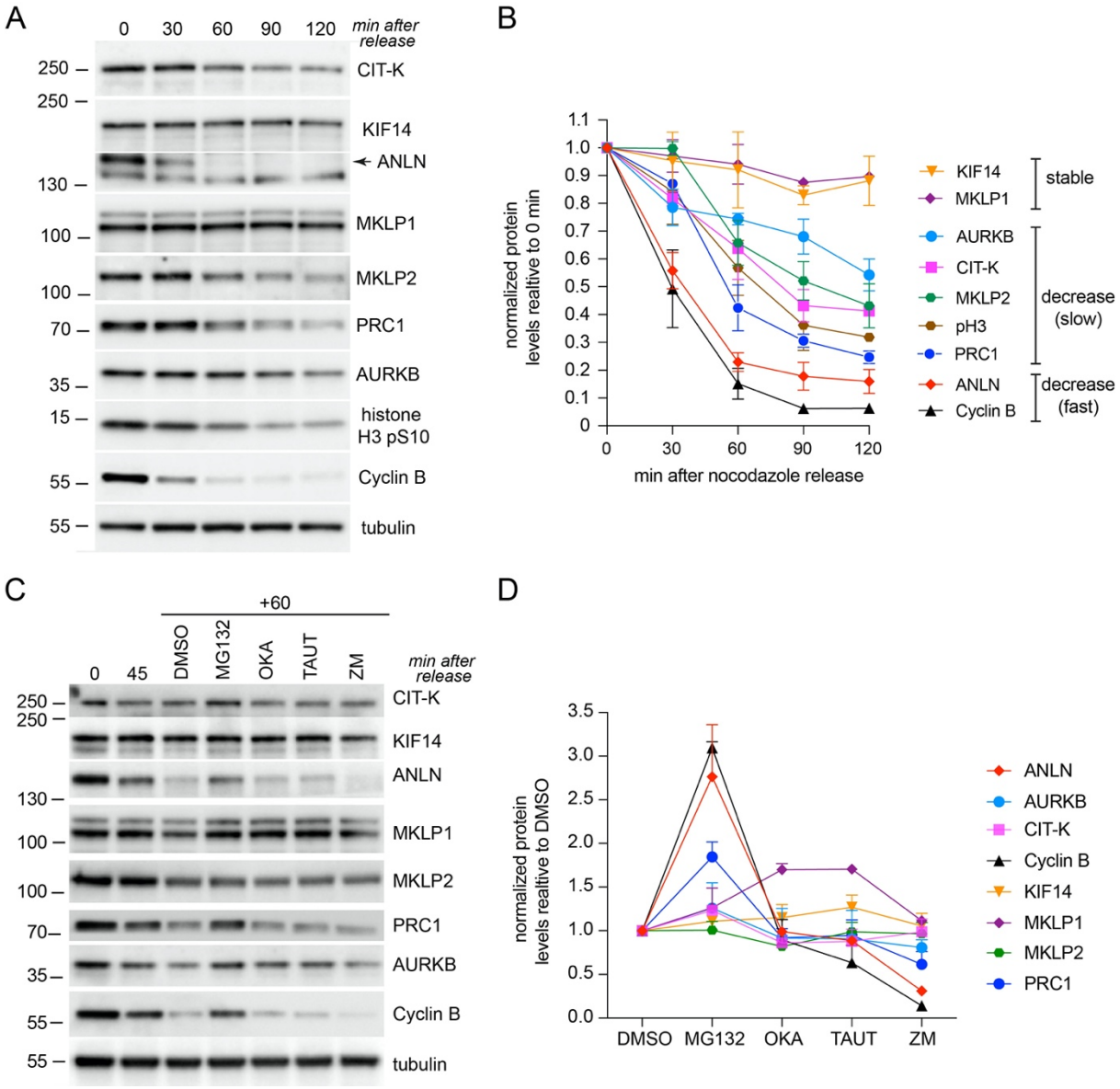

Figure 2. Different expression profiles of midbody proteins during mitotic exit. (A) Time course analysis of midbody protein expression during mitotic exit. HeLa cells were synchronized by thymidine/nocodazole block and then collected at the indicate time points after nocodazole release. Proteins were extracted and used in Western blot analysis to identify the antigens indicated to the right. The numbers on the left indicate the sizes of the molecular mass marker. (B) Graph showing the quantification of protein levels, normalized to tubulin and relative to levels at time 0 min, from at least two different western blots like the one shown in (A) using protein extracts from two separate experiments. (C) Effect of different inhibitors on midbody protein levels. HeLa cells were synchronized by thymidine/nocodazole block, released for 45 min in fresh medium, and then incubated for further 60 min in MG132, okadaic acid (OKA), tautomycetin (TAUT), ZM447439 (ZM), or the solvent DMSO as control. Proteins were extracted and used in Western blot analysis to identify the antigens indicated to the right. The numbers on the left indicate the sizes of the molecular mass marker. (D) Graph showing the quantification of protein levels, normalized to tubulin and relative to DMSO levels, from at least two different western blots like the one shown in (C) using protein extracts from two separate experiments.

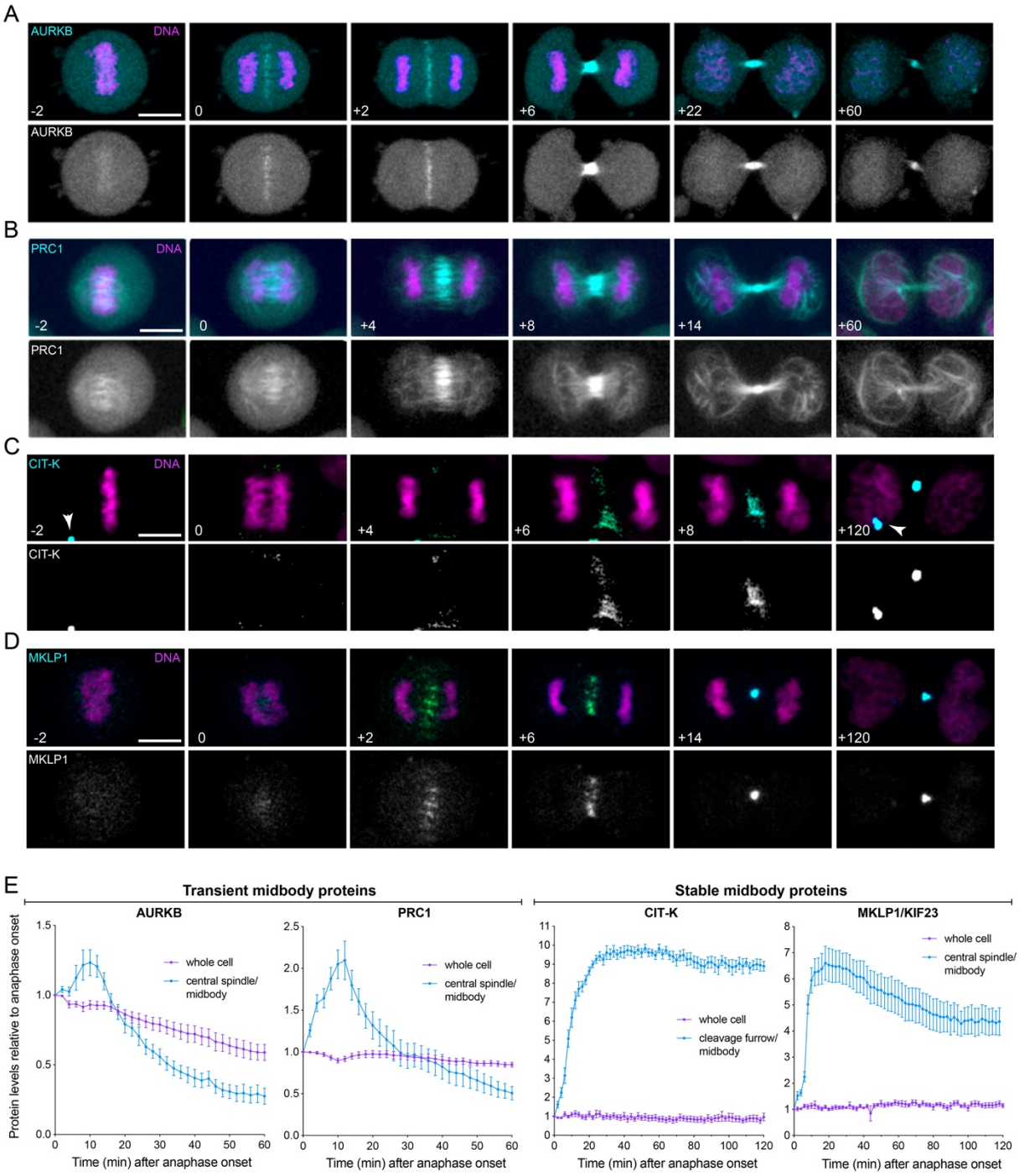

Figure 3. Midbody proteins display distinct dynamics during cytokinesis. (A-D) Selected images from time-lapse recordings of HeLa cells expressing GFP-tagged AURKB (A), PRC1 (B), CIT-K (C) and KIF23/MKLP1 (D). Chromosomes were visualised using SiR-DNA. GFP-tagged proteins are in cyan and DNA in magenta in the merged panels. Time is in minutes relative to anaphase onset (0 time point). The arrowheads in (C) marks CIT-K::GFP localization to post-mitotic midbodies. Bar, 10 µm. (E) Quantification of midbody proteins during cytokinesis. Fluorescence intensity values were measured in whole cells and at the central spindle/cleavage furrow/midbody and then normalized relative to the anaphase onset (0) time point. Bars indicate SEM, n=10.

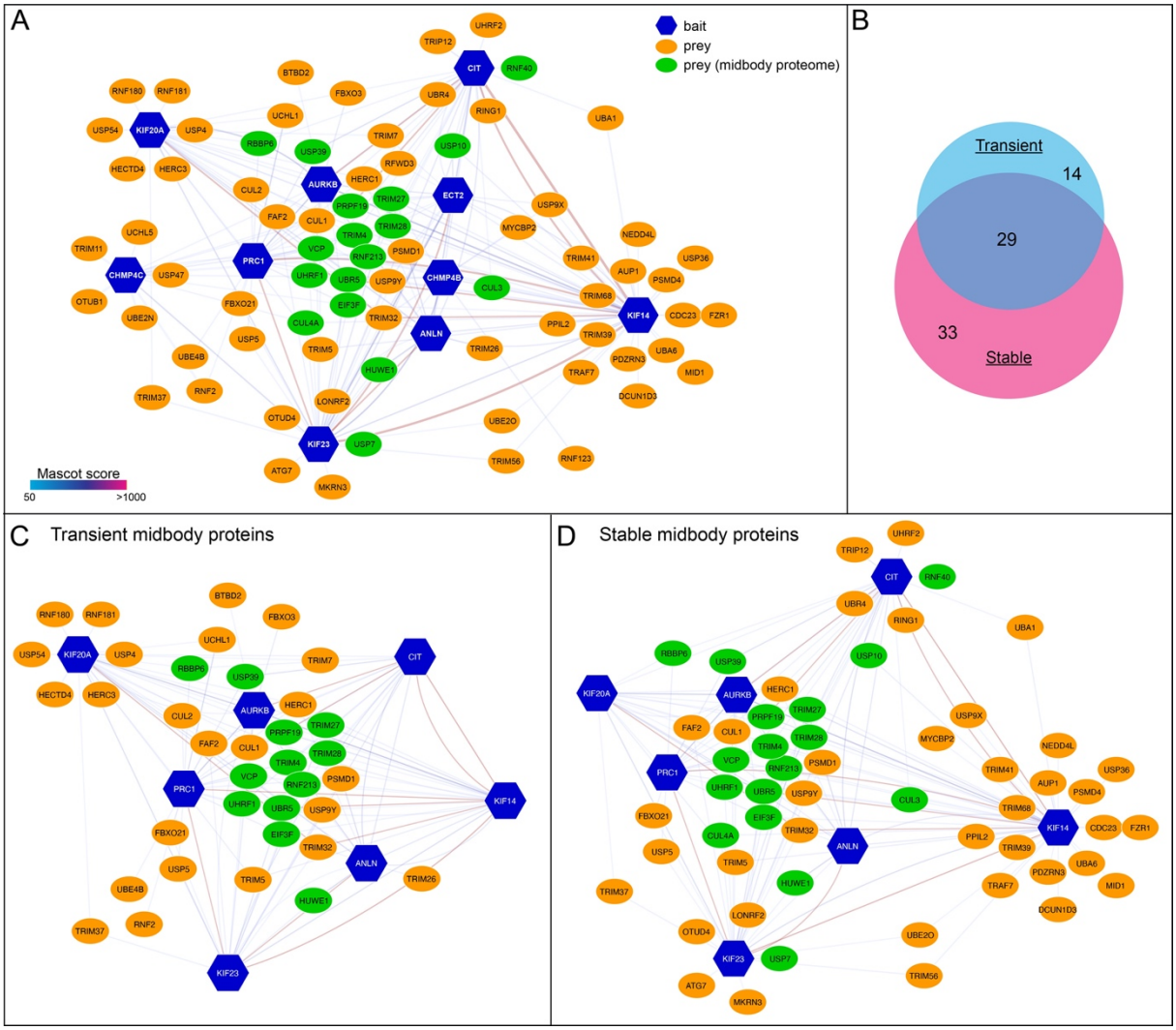

Figure 4. (A) Diagram illustrating the midbody ubiquitylation interactome. Baits are indicated with blue hexagons, while preys are represented as ovals, either in green, if they were also found in the midbody proteome, or in orange. The edges connecting the network nodes are colored according to their Mascot scores as indicated in the color scale bar at the bottom left (see also [11]). Preys shared by multiple baits are clustered in the center. (B) Proportional Venn diagram showing the number of proteins present in the transient and stable midbody ubiquitylation interactomes. (C-D) Diagrams illustrating the midbody ubiquitylation interactomes generated using either transient (C) or stable (D) midbody proteins as baits. Baits, preys and edges are as in (A).